Contact guidance requires spatial control of leading-edge protrusion

G. R. Ramirez-San Juan[a,b,c,d], P. W. Oakes[b,c,d,e,f], and M. L. Gardel[b,c,d,*]
[a]Graduate Program in Biophysical Sciences, [b]Institute for Biophysical Dynamics, [c]James Franck Institute, and [d]Department of Physics, University of Chicago, Chicago, IL 60637; [e]Department of Physics and Astronomy and [f]Department of Biology, University of Rochester, Rochester, NY 14627

ABSTRACT **In vivo, geometric cues from the extracellular matrix (ECM) are critical for the regulation of cell shape, adhesion, and migration. During contact guidance, the fibrillar architecture of the ECM promotes an elongated cell shape and migration along the fibrils. The subcellular mechanisms by which cells sense ECM geometry and translate it into changes in shape and migration direction are not understood. Here we pattern linear fibronectin features to mimic fibrillar ECM and elucidate the mechanisms of contact guidance. By systematically varying patterned line spacing, we show that a 2-μm spacing is sufficient to promote cell shape elongation and migration parallel to the ECM, or contact guidance. As line spacing is increased, contact guidance increases without affecting migration speed. To elucidate the subcellular mechanisms of contact guidance, we analyze quantitatively protrusion dynamics and find that the structured ECM orients cellular protrusions parallel to the ECM. This spatial organization of protrusion relies on myosin II contractility, and feedback between adhesion and Rac-mediated protrusive activity, such that we find Arp2/3 inhibition can promote contact guidance. Together our data support a model for contact guidance in which the ECM enforces spatial constraints on the lamellipodia that result in cell shape elongation and enforce migration direction.**

Monitoring Editor
Paul Forscher
Yale University

Received: Nov 8, 2016
Revised: Jan 26, 2017
Accepted: Feb 17, 2017

INTRODUCTION

Cell migration plays a central role in several developmental, physiological, and pathological processes. During development, directed migration is required for diverse morphogenetic processes conserved among organisms, ranging from branching morphogenesis of kidney and breast tissue, to migration of neural crest cells out of the tube (Keller, 2005; Vasilyev *et al.*, 2009; Brownfield *et al.*, 2013). In adults, leukocytes are required to translocate to areas of insult to mediate phagocytic and immune function (Luster *et al.*, 2005). Migration of fibroblasts and vascular endothelial cells is essential for wound healing (Gillitzer and Goebeler, 2001). In cancer metastasis, multicellular masses invade their extracellular matrix (ECM) and migrate into the bloodstream (Friedl and Gilmour, 2009). Migration of single cells has been studied extensively and is relatively well understood. Despite its complexity, cell migration can be thought of as consisting of four discrete steps: protrusion of the cell's leading cell edge, adhesion to the ECM, generation of traction stresses against adhesions, and release of rear adhesions and cell body contraction (Gardel *et al.*, 2010). To get productive advancement, cells must first polarize to form a leading front and a back. The ability of cells to polarize is controlled by numerous external and internal cues. Internally, membrane tension can restrict competing growing leading edges (Houk *et al.*, 2012), and regions of high Rho activity can inhibit cell protrusion (Wang *et al.*, 2003), whereas externally, physical characteristics of the ECM such as rigidity, density, and geometry can induce cell polarity, including directed migration and elongation of cell shape (Petrie *et al.*, 2009; Charras and Sahai, 2014).

Decades of work have shown that changes in geometry, or spatial arrangement, of adhesive cues provided by the ECM can align cell shape and guide cell motility (Weiss and Garber, 1952; Dunn and Ebendal, 1978; Clark *et al.*, 1990; den Braber *et al.*, 1996a;

This article was published online ahead of print in MBoC in Press (http://www.molbiolcell.org/cgi/doi/10.1091/mbc.E16-11-0769) on February 22, 2017.

*Address correspondence to: M. L. Gardel (gardel@uchicago.edu).

Abbreviations used: ECM, extracellular matrix; GEF, guanine nucleotide exchange factor; GFP, green fluorescent protein; PAK, p21-activated kinase; ROCK, Rho kinase; WT, wild type.

Teixeira *et al.*, 2003; Provenzano *et al.*, 2008; Xia *et al.*, 2008). During this process, termed contact guidance, the geometry of the ECM enforces changes to cell morphology and migration direction (Petrie *et al.*, 2009; Reig *et al.*, 2014). Classical studies in vivo and in vitro have shown that cells interacting with fibrillar ECM networks exhibit contact guidance (Weiss and Garber, 1952; Dunn and Heath, 1976; Dunn and Ebendal, 1978). For instance, during amphibian gastrulation, aligned ECM fibrils facilitate mesodermal cell migration toward the animal pole (Nakatsuji *et al.*, 1982), whereas cells interacting with fibrin clots reorient the ECM, which in turn alters their morphology and migration (Weiss and Garber, 1952).

Micropatterning has been a powerful tool to demonstrate that changes in the geometrical presentation of ligands alone, such as area, shape, and density, can regulate cell shape and migration (Clark *et al.*, 1990; den Braber *et al.*, 1996a; Teixeira *et al.*, 2003; Provenzano *et al.*, 2008; Xia *et al.*, 2008; Doyle *et al.*, 2009; Yoon *et al.*, 2012; Londono *et al.*, 2014). Significantly less explored are the subcellular mechanisms used by cells to sense changes in ECM geometrical parameters. In patterned environments, lamellipodia and fillipodia extend parallel to the ECM (Teixeira *et al.*, 2003, 2006). Extension of lamellipodia parallel to the ECM has been correlated with localized Rac activity at adhesions (Xia *et al.*, 2008) and actin polymerization parallel to the ECM (Sun *et al.*, 2015), whereas inhibition of myosin II contractility has been shown to be important to maintain cell shapes in response to ECM architecture (Frey *et al.*, 2006; Spedden *et al.*, 2014). In these studies, along with ECM orientation, density of available ECM (Xia *et al.*, 2008) and surface topography (Frey *et al.*, 2006; Spedden *et al.*, 2014; Sun *et al.*, 2015) were varied, making it impossible to discern effects of ECM alignment alone. Given that the ECM in vivo typically comprises a network of fibers with micrometer-scale structure (Nakatsuji *et al.*, 1982; Condeelis and Segall, 2003; Baker and Chen, 2012), we sought to understand the mechanism by which interfibrillar spacing controls the tendency of cells to align and move along fibrils.

RESULTS

Contact guidance can be tuned by micrometer-scale changes in ECM geometry

To mimic fibrillar geometry and isolate the effects of variations in interfibrillar spacing, we micropatterned parallel lines of fibronectin of a constant width (2 μm) with interline spacing varying from 0 (uniform) to 10 μm (Oakes *et al.*, 2014). These dimensions were chosen such that NIH 3T3 fibroblasts were able to spread on multiple lines, and the line width was large enough for typical focal adhesion formation (Lehnert *et al.*, 2004; Doyle *et al.*, 2009). Fibronectin was patterned onto polyacrylamide gels with a stiffness that allowed for optimal fibroblast migration (Lo *et al.*, 2000). Immunofluorescence of fibronectin, paxillin, and actin confirmed that focal adhesions were excluded from unpatterned regions and formed on fibronectin stripes, allowing cells to attach to several pattern features (Figure 1, A and B).

Fibroblasts plated on uniformly coated substrates (0-μm spacing) acquired a characteristic polarized morphology with no preferred

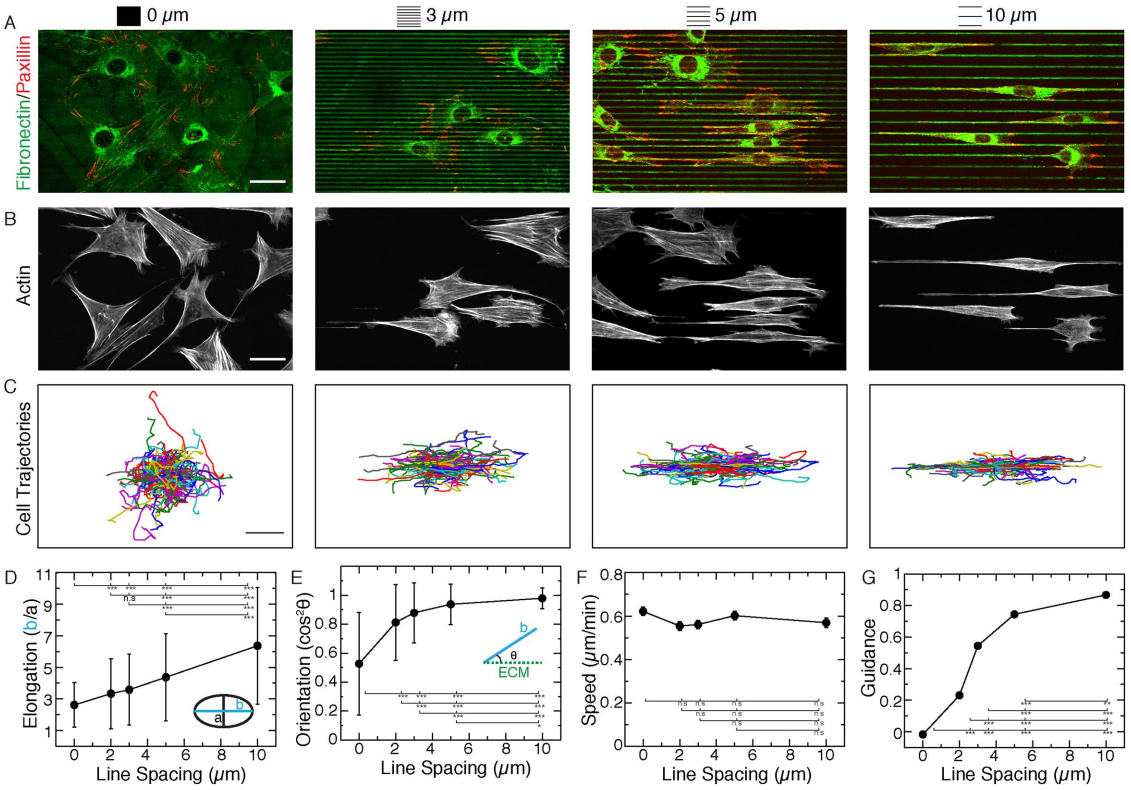

FIGURE 1: (A, B) Fluorescence images of paxillin, fibronectin, and F-actin of NIH 3T3 fibroblasts plated on uniform (0 μm) and linear ECM geometries. ECM patterns consist of 2-μm-wide stripes spaced at 3, 5, and 10 μm, respectively. Scale bar, 30 μm. (C) Migration trajectories of cells on uniform (0 μm) and linear ECM spaced at 3, 5, and 10 μm, respectively. (D–G) Cell elongation, orientation, instantaneous speed, and guidance as a function of ECM line spacing. Elongation is measured by taking the ratio of long over short cellular axes. Orientation is determined by measuring the angle, θ, between the long axis of the cell and a line parallel to the ECM and calculating the orientation parameter, $P = \cos^2\theta$. Guidance for $\tau = 300$ min is plotted. Mean and SD for >100 cells are shown for each condition. Insets, results of pairwise statistical testing: *$p \leq 0.05$, **$p \leq 0.01$, ***$p \leq 0.001$ (see Supplemental Table S3 for exact p values).

directional orientation (Mogilner and Keren, 2009). On all line patterns, cells elongated and became preferentially aligned to the ECM (Figure 1B). To quantify these changes in shape and orientation, we fitted an ellipse to each cell and characterized the elongation as the ratio between the long and short axes, with the alignment to the axis defined by the ECM lines with the parameter $P = \cos^2\theta$, where θ is the angle between a line parallel to the ECM and the long axis of the cell ellipse. Cell elongation increased linearly with line spacing (Figure 1D), whereas cell spread area decreased (Supplemental Figure S1A). Orientation increased sharply from 0- to 2-μm spacing, with a mean orientation with respect to the ECM lines of 0.81 out of a maximum possible value of 1. The orientation between 2 and 10 μm then slowly increased until it reached a mean value of 0.98, indicating almost complete alignment with the ECM (Figure 1E). Thus increased fibril spacing promoted an elongated cell morphology, with the long axis parallel to the line direction.

During cell migration, the long axis typically defines the axis of front–back polarity and corresponds to the direction of migration (Lauffenburger and Horwitz, 1996; Petrie *et al.*, 2009). Thus we next sought to determine how these changes in ECM presentation affected the speed and direction of spontaneous cell migration. Figure 1C shows rose plots of the trajectories of ~100 cells during a period of 10 h. Strikingly, the instantaneous migration speed was unaffected over this range of line spacings (Figure 1F), but the cell trajectories became oriented parallel to the ECM with increased line spacing (Figure 1C and Supplemental Movie S1). To quantify this effect, we defined a binary guidance (Londono *et al.*, 2014) that measured the orientation of a cell's trajectory relative to the ECM. Briefly, we calculated the angle θ between the displacement vector of a cell and the ECM and defined binary guidance, g, such that $g(t) = 0$ if $\theta > 25$ and $g(t) = 0$ if $\theta \leq 25$. When we averaged this measurement over several time intervals τ, we obtained a guidance parameter $G(\tau) = \sum_{t=t_i}^{t_i+\tau} g(t)/\tau$, which represents accurately the direction of a cell's trajectory over different time scales (Supplemental Figure S1B). The value of G at $\tau = 300$ min is reported because it is the relevant time scale for the experiments performed. The guidance parameter demonstrates that migration direction is increasingly parallel to the ECM as a function of line spacing, having its sharpest increase from 2 to 3 μm (Figure 1G). Consistent with the changes observed in cell migration and cell shape, cells oriented their traction stresses and migration direction parallel to the ECM on line patterns (Supplemental Figure S1).

Taken together, these results demonstrate that micrometer-scale variations in fibril-like spacing from 2 to 3 μm can tune cell shape and bias the direction of cell migration parallel to the ECM. This is consistent with previous studies, which found that micrometer-scale changes in pattern spacing can induce cell shape alignment (Clark *et al.*, 1990; den Braber *et al.*, 1996a; Teixeira *et al.*, 2003; Xia *et al.*, 2008). However, in these studies, along with line spacing, size of adhesive regions (Xia *et al.*, 2008) or surface topography was varied (Clark *et al.*, 1990; den Braber *et al.*, 1996b; Teixeira *et al.*, 2003), making it impossible to discern the effects of line spacing alone.

Leading-edge protrusions are oriented parallel to the ECM on line patterns via myosin II contractility and ECM feedback

Cell migration is controlled by the spatiotemporal organization of leading-edge protrusion, adhesion, and cell retraction (Gardel *et al.*, 2010). To investigate how protrusion dynamics were altered during contact guidance, we followed shape changes in cells transfected with a fluorescent membrane marker (green fluorescent protein [GFP]–stargazin) that facilitated the identification of the cell edge (Figure 2A, Supplemental Figure S2A, and Supplemental Movie S2). From the cell contours, we identified the area and orientation of protrusive regions (Figure 2B). We found that the area of individual protrusions was unaffected by changes in line spacing (Figure 2C). However, as the line spacing increased, protrusions became oriented with respect to the ECM lines (Figure 2D). This result suggested that changes in ECM line spacing most significantly affected the spatial organization of protrusions rather than their overall size. This is consistent with our observation that contact guidance is promoted even at line spacings of 2–3 μm that would not prevent the stabilization of lamellipodial protrusions.

The spatial organization of lamellipodial activity is controlled by numerous intracellular and extracellular cues (Raftopoulou and Hall, 2004; Charras and Sahai, 2014). Most relevant to this work are the well-established feedbacks between cell shape (Parker *et al.*, 2002; James *et al.*, 2008; Gabella *et al.*, 2014; Elliott *et al.*, 2015) and cell–matrix adhesion to local protrusive activity (Nayal *et al.*, 2006; Xia *et al.*, 2008). The feedback between cell shape and protrusion regulation is mediated by myosin II contractility. Along the long, nonadherent edges of cells, myosin II–mediated contractility suppresses local protrusive activity (Elliott *et al.*, 2015). At focal adhesion sites, positive feedback between cell–matrix adhesion and protrusive activity is achieved by activation of Rac through β-pix–mediated focal adhesion signaling (Nayal *et al.*, 2006).

To explore whether the elongated shape plays an important role in the spatial organization of protrusion we observe, we analyzed spreading and protrusion dynamics in the initial stages of cell spreading. On uniformly coated substrates, cells undergo rapid and Rac1-mediated isotropic spreading after initial attachment (Price *et al.*, 1998; Wolfenson *et al.*, 2014). By contrast, cells spread anisotropically on line patterns (Figure 2E, left, and Supplemental Movie S3, top) and quickly oriented along linear features within 4 min after initial contact (Figure 2G). After the initial orientation, cell elongation continued to increase (Figure 2F) even after cells had reached their maximum spread area (Supplemental Figure S2B). The rapid orientation of cell shape on ECM attachment suggests that positive feedback with the ECM may be sufficient to guide protrusion dynamics even in the absence of myosin II–mediated regulation. To determine the role of myosin II activity in the ability of cells to orient along ECM lines during initial spreading, we observed spreading dynamics in cells treated with 20 μM of the Rho kinase (ROCK) inhibitor Y-27632. Surprisingly, ROCK-inhibited cells failed to elongate during spreading on all line spacings (Figures 2, E, right, and F, and Supplemental Movie S3, bottom). Furthermore, cells had severe defects orienting parallel to the ECM (Figure 2G), achieving orientation only at 10-μm spacing at later times during spreading, showing that ROCK-mediated contractility is necessary to direct protrusions parallel to the ECM, even in the earliest stages of cell–ECM attachment.

These results demonstrate that structured ECM regulates protrusive activity spatially to enforce cell shape polarization along the axis of the ECM lines. The altered local density of ECM did not affect the overall protrusion size but biased their formation preferentially along the ECM axis even at spacings of 2–3 μm. Because lamellipodia are large enough to span those gap sizes (Machacek *et al.*, 2009), this suggests that contact guidance can occur even when the size of the protrusions enables them to span line spacings. However, because protrusion area remains constant across spacings (Figure 2C), it is possible that limitations on the size of protrusions can bias their direction, particularly at spacings >3 μm. We find that spatial control of protrusive activity is regulated from the earliest stages of cell

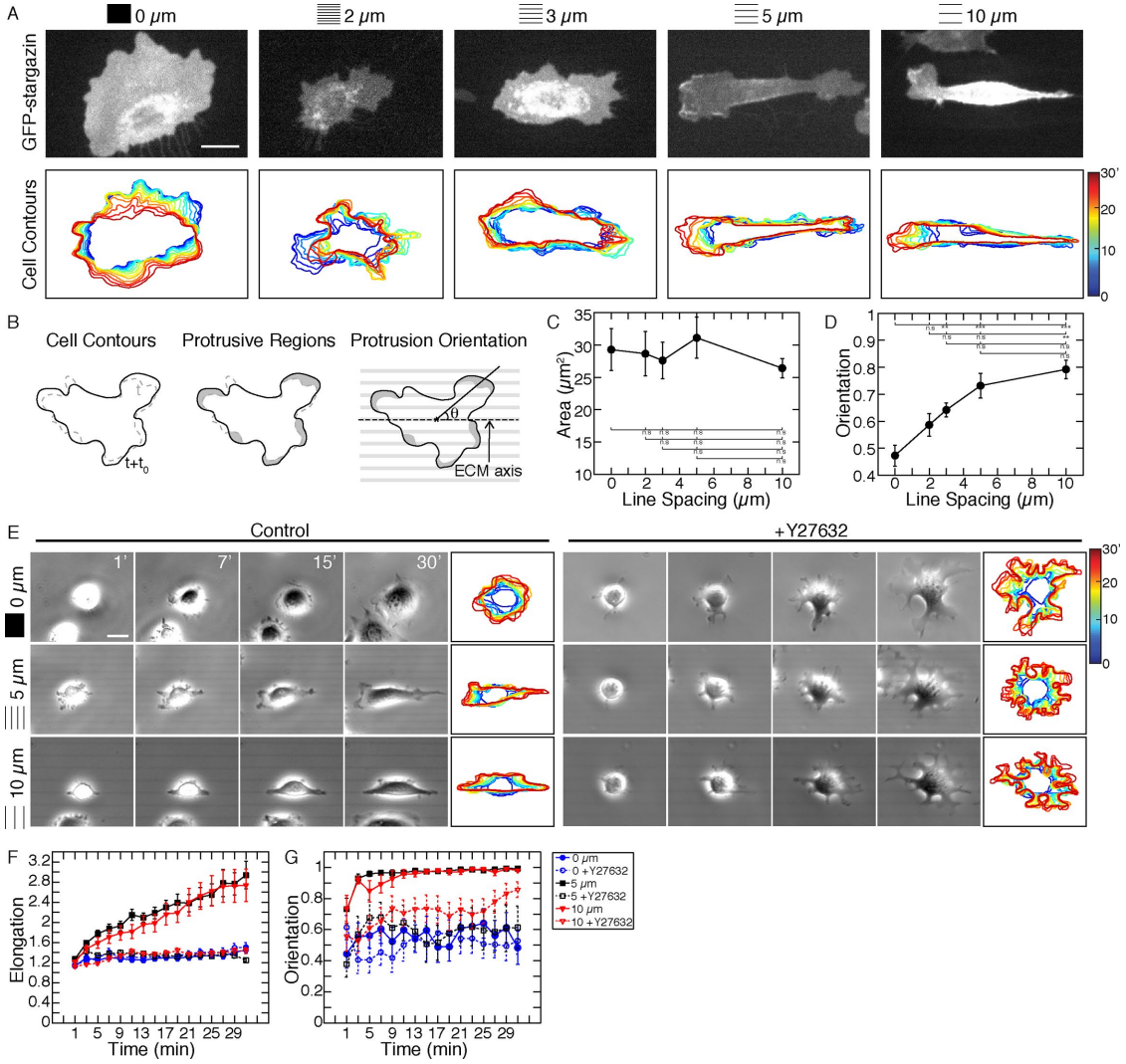

FIGURE 2: (A) GFP-stargazin images of cells on linear ECM patterns with uniform (0 μm) and 2-, 3-, 5-, and 10-μm line spacings. Contour plots show cell outlines obtained every 1 min over 30 min. (B) Schematic representation of analysis of leading-edge protrusions. From cell contours at time t and $t + t_0$ (left), areas of leading-edge growth are identified as protrusions (middle). Protrusion orientation is found by measuring the angle between a line connecting the protrusion center with the cell center and a line parallel to the ECM. Final orientation values are obtained by calculating the orientation parameter, $P = \cos^2\theta$. (C, D) Area and orientation of cell protrusion as a function of ECM line spacing. Mean and SEM for ≥12 cells. Insets, results of pairwise statistical testing: $*p \le 0.05$, $**p \le 0.01$, $***p \le 0.001$ (see Supplemental Table S3 for exact p values). (E) Phase-contrast images of NIH 3T3 fibroblasts spreading on uniform (0 μm) and ECM striped patterns spaced at 5 and 10 μm, respectively. Images correspond to 1, 5, 10, 15, and 30 min; contour plots show the entire time lapse. Left, control cells treated with dimethyl sulfoxide (DMSO); right, cells treated with 20 μM Y-27632. Scale bar, 20 μm. (F, G) Cell elongation and orientation during cell spreading for uniform (blue), 5-μm (black), and 10-μm (red) patterns. DMSO- and Y-27632–treated cells are shown by closed and open symbols, respectively. Data are presented as the mean and SD for ≥15 cells.

spreading. ROCK-mediated contractility is necessary to achieve cell shape polarization during spreading, suggesting that it plays an important role in contact guidance, which is consistent with its known role providing cytoskeletal coherence during spreading (Cai *et al.*, 2010).

ROCK-mediated contractility is necessary for contact guidance

Because ROCK-mediated contractility was required to polarize cells during spreading, we next explored its role in contact guidance. We first analyzed the shape of fully spread cells after treatment with ROCK inhibitor for 45 min (Figure 3A, top). Consistent with the characteristic morphology of ROCK-inhibited cells, cells often had multiple protrusive fronts and a tail retraction defect (Figure 3A, top; Omelchenko *et al.*, 2002). In contrast to control cells, ROCK-inhibited cells did not elongate further when placed on line patterns (Figure 3E and Supplemental Figure S3A, top). However, ROCK-inhibited cells exhibited a similar tendency to orient along the line axis to control cells (Figure 3, A, top, and F). Despite this orientation, migration directionality was severely affected in ROCK-inhibited cells (Figure 3A, bottom, Supplemental Figure S3A, bottom, and Supplemental Movie S4).

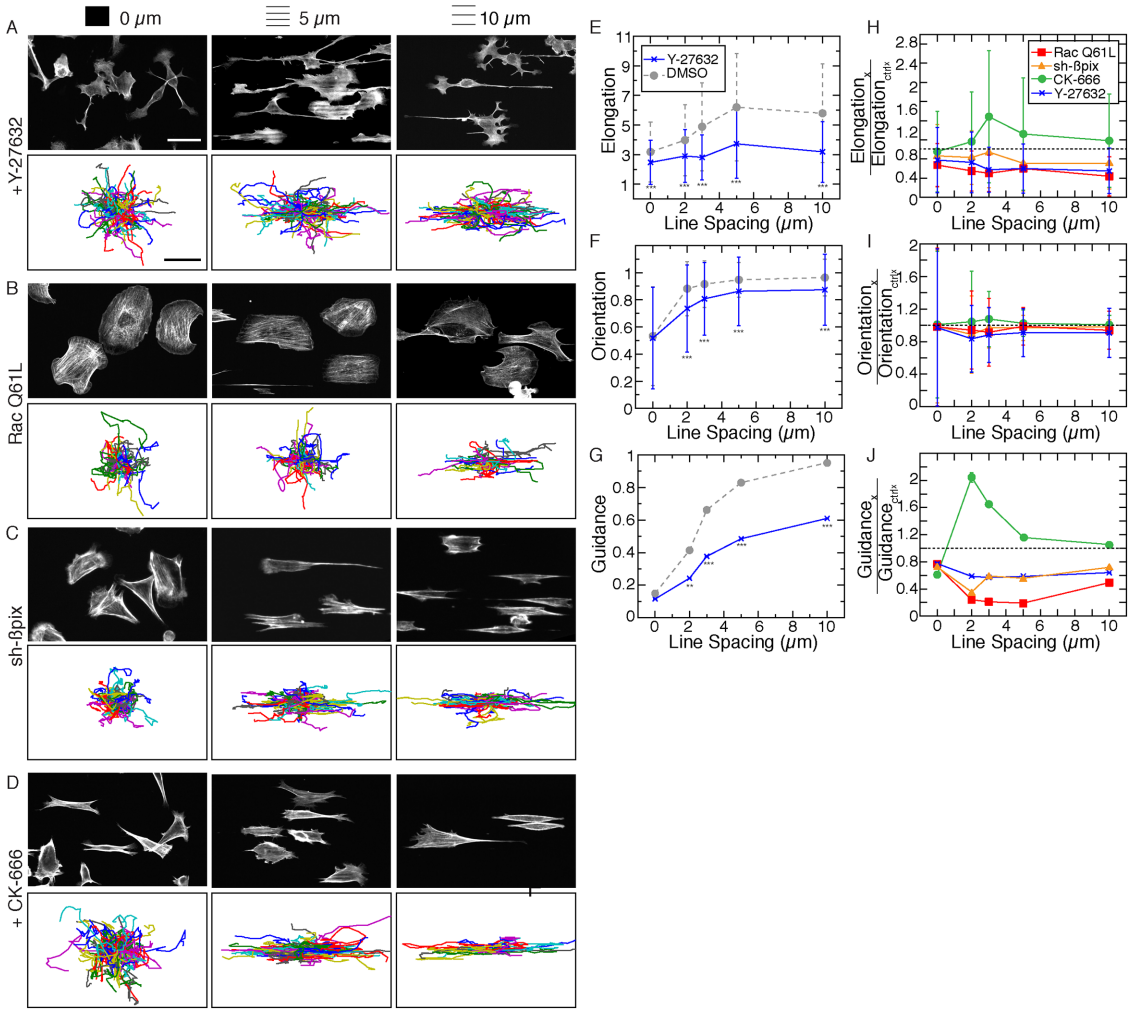

FIGURE 3: (A, D) Top, F-actin cells on patterns treated with 20 μM Y-27632 (A), transfected with RacQ61L (B), an shRNA to β-pix (C), or treated with 100 μM CK-666 (D). Bottom, migration trajectories for cells in these conditions over 10 h. (E–G) Cell elongation, orientation, and guidance as a function of line spacing for cells treated with 20 μM Y-27632 (solid line). Light gray symbols and dotted line show data for cells treated with DMSO. *$p \leq 0.05$, **$p \leq 0.01$, ***$p \leq 0.001$, *t* tests (see Supplemental Table S3 for exact *p* values). (H–J) Fold change in elongation, orientation, and guidance of cells with pharmacological or genetic perturbations: RacQ61L, shRNA β-pix, 100 μM CK-666, or 20 μM Y-27632. All data are plotted as a ratio with respect to their controls: WT, shNT, CK-689, or DMSO, respectively.

Compared to control cells, the guidance was reduced by 50% (Figure 3, G and J). Thus inhibition of ROCK-mediated contractility results in a decoupling between cell orientation and guidance.

To determine the mechanisms causing the migration guidance defect in ROCK-inhibited cells, we analyzed protrusions using the method described earlier. Consistent with known effects of ROCK inhibition (Omelchenko *et al.*, 2002), cells had disorganized protrusions and poorly defined leading-edge fronts (Figure 4A, Supplemental Figure S4A, and Supplemental Movies S8 and S9). Protrusion area doubled relative to controls for spacings <10 μm (Figure 4, E and G). More strikingly, protrusions failed to organize parallel to the ECM, as shown by a sharp decrease in orientation for line spacings <10 μm (Figure 4F). Compared to control cells, the orientation of protrusions decreased by 20% (Figure 4H).

Together these results show that ROCK-mediated contractility is necessary to organize protrusions spatially in response to structured ECM, promoting contact guidance. Previous work suggested that inhibition of myosin II contractility reduced the ability of cells to orient parallel to the ECM surface microtopography and nanotopography (Frey *et al.*, 2006; Spedden *et al.*, 2014). Our results demonstrate that the mechanism is likely through the important role of ROCK-mediated contractility in spatial organization of protrusions (Lo *et al.*, 2004).

Perturbations to protrusive activity via misregulation of Rac 1 impair contact guidance

Spatial regulation of Rac activity controls the formation, growth, and size of leading-edge protrusions (Nobes and Hall, 1999; Ridley *et al.*, 2003; Pankov *et al.*, 2005; Machacek *et al.*, 2009). High levels of Rac activity were previously shown to impede directed migration by promoting the formation of several lamellipodial fronts (Pankov *et al.*, 2005). Therefore, to promote global activation of Rac and disrupt the spatial regulation of lamellipodia formation, we expressed the constitutively active form RacQ61L. RacQ61L cells were rounder (Figure 3B top, and Supplemental Figure S3D), as shown by the 50% decrease in elongation for all line spacings relative to wild-type (WT) cells (Figure 3H). Elongation values in these cells were >1, allowing us to define a long axis to measure cell shape orientation

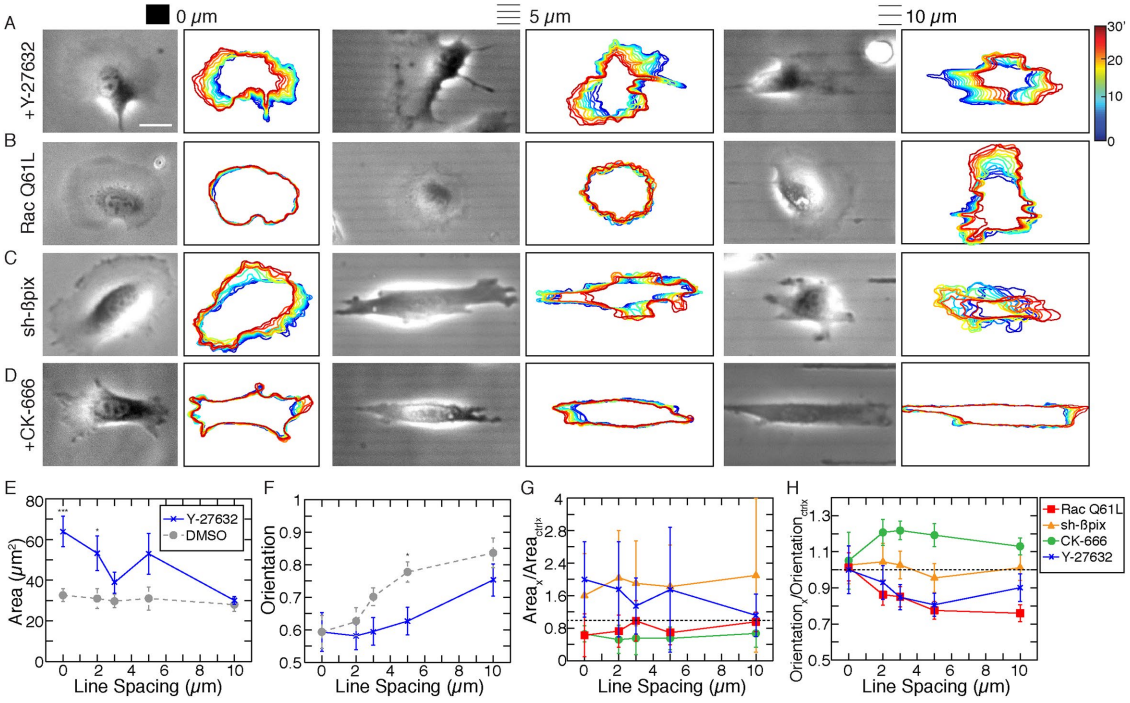

FIGURE 4: (A–D) Phase contrast images of cells with specified perturbations on uniform and 5- and 10-μm patterns. Contour plots show cell outlines for a 30-min time interval during migration. Cells shown were treated with 20 μM Y-27632 (A), transfected with RacQ61L (B), shRNA to β-pix (C), or treated with 100 μM CK-666 (D). Scale bar, 30 μm. (E, F) Area and orientation of protrusions as a function of ECM line spacing for cells treated with 20 μM Y-27632 (solid line). Gray data points and dashed line are for control cells treated with DMSO. Mean and SEM for ≥8 cells. $*p \leq 0.05$, $**p \leq 0.01$, $***p \leq 0.001$, *t* tests (see Supplemental Table S3 for exact *p* values). (G, H) Fold change in area and orientation of individual protrusions as a function of ECM line spacing for cells transfected with RacQ61L, shRNA to β-pix, treated with 100 μM CK-666, or 20 μM Y-27632 relative to their respective controls: WT, shNT, CK-689, or DMSO.

(Supplemental Figure S3D). Intriguingly, orientation values in RacQ61L cells were comparable to those in WT cells (Supplemental Figure S3E), as shown by the ratio between the values being close to 1 (Figure 3I). In contrast, migration trajectories were no longer parallel to the ECM (Figure 3B, bottom, and Supplemental Movie S5), except at 10-μm line spacing, where cells exhibited limited guidance (Supplemental Figure S3F). The defect in guidance was more pronounced than for ROCK-inhibited cells, because for all line spacings, guidance in RacQ61L cells was reduced by at least 50% (Figure 3J).

To determine how protrusive activity was altered in cells expressing RacQ61L, we next measured area and localization of leading-edge protrusion. First, we noticed that cells exhibited protrusions around the entire cell body (Figure 4B and Supplemental Movie S10). Measurements showed that protrusion areas were comparable to those in WT cells (Figure 4G and Supplemental Figure S4D). By contrast, protrusions failed to orient parallel to the ECM as a function of line spacing (Supplemental Figure S4E), decreasing in orientation by 30% relative to WT cells (Figure 4H). This trend of protrusion orientation mimics the trend observed for guidance (compare Figures 3J and 4H), suggesting that the ability of cells to migrate parallel to the ECM relies on biasing protrusive activity in the direction parallel to the lines.

Another major regulator of protrusive activity relevant to our context is the positive feedback between sites of new adhesion and protrusion formation, controlled by p21-activated kinase (PAK)–mediated changes in paxillin phosphorylation, which recruits the Rac guanine nucleotide exchange factor (GEF) β-pix (Nayal *et al.*, 2006). Knockdown of β-pix has been linked to increased lamellipodia protrusion and defects in directed migration (Kutys and Yamada, 2014; Omelchenko *et al.*, 2014). To explore how disruption to this feedback affected contact guidance, we knocked down β-pix to 30% of its endogenous levels (Supplemental Figure S3M). For cells on lines, β-pix knockdown (KD) led to a slight reduction in elongation for line spacings >3 μm (Figure 3C, top, and Supplemental Figure S3B, top), reaching only 70% of the nontargeting-control (NT) cell values (Figure 3H and Supplemental Figure S3G).

Similar to previously analyzed cells, β-pix KD had minimal defects in cell orientation parallel to the ECM (Figure 3I and Supplemental Figure S3H). Strikingly, migration guidance was reduced in these cells by ~50% compared with the NT-control cells (Figure 3J, Supplemental Figure S3I, and Supplemental Movie S6). Together these results show that β-pix feedback between adhesion and protrusion initiation is not essential for cell shape anisotropies during contact guidance; however, it plays an important role in directing migration in the direction of the ECM. Because β-pix is required for the positive feedback between adhesion and protrusion, we expected β-pix KD cells to mislocalize protrusions similarly to RacQ61L cells. Surprisingly, cell protrusions occurred mostly along the ECM axis (Figure 4C, Supplemental Figure S4B, and Supplemental Movies S11 and S12). Quantification of protrusion orientation revealed that protrusions localized parallel to the ECM to levels comparable to that for NT control cells (Figure 4H and Supplemental Figure S4G). In contrast with RacQ61L cells, β-pix KD cells had large protrusions that fluctuated greatly in size, as evidenced by the twofold increase in protrusion area and the large fluctuations in this measurement (Figure 4G and Supplemental Figure S4F).

Taken together, these results show that spatial regulation of protrusive activity is required for contact guidance. Of importance, in each of these phenotypes, the guidance can be significantly affected without much change to alignment of the cell long axis in the directions of the lines. Our β-pix KD data suggest that in addition to localization of protrusions, the size of protrusions can regulate the directed migration for cells on patterns. This supports our previous hypothesis in which the size of protrusions can limit the ability of cells to migrate perpendicular to the ECM. To further test this idea, we decided to explore in detail whether changes to protrusion size could affect contact guidance.

Arp2/3 inhibition increases contact guidance

The Arp2/3 complex is an essential component of lamellipodial protrusions at the leading edge (Wu *et al.*, 2012; Beckham *et al.*, 2014). Previous work showed that lamellipodia-driven migration plays an important role in haptotaxis (Wu *et al.*, 2012; King *et al.*, 2016), suggesting that it also might also impede contact guidance. To explore this, we treated cells with 100 μM Arp2/3 inhibitor CK-666. On first inspection, Arp 2/3-inhibited cells appeared to be more elongated and polarized in the direction of the ECM (Figure 3D, top, and Supplemental Figure S3C, top). Quantification confirmed that these cells had increased elongation compared with cells treated with the control molecule CK-689, particularly at line spacings <5 μm (Figure 3H and Supplemental Figure S3J), whereas cell orientation was only slightly higher than for controls (Figure 3I and Supplemental Figure S3K). Of greater significance, we observed higher values for guidance at all line spacings, with a twofold increase at spacings <5 μm compared with controls (Figure 3J, Supplemental Figure S3L, and Supplemental Movie S7). These measurements provide the first observation of an increase in guidance compared with control cells.

Our previous results show that contact guidance depends inversely on protrusion size and directly on localization of protrusions parallel to the ECM. We therefore expected Arp 2/3-inhibited cells to have reduced protrusion size and/or highly localized protrusions. Indeed, cell protrusions appeared to be smaller and directed almost exclusively in the direction of the ECM (Figure 4D, Supplemental Figure S4C, and Supplemental Movies S13 and S14). Quantitative analysis confirmed that protrusions in Arp2/3-inhibited cells decreased by 40% in area compared with cells treated with the control molecule (Figure 4G and Supplemental Figure S4H). Remarkably, orientation of protrusions followed the same trend as migration guidance, increasing 1.2-fold for cells on line spacings <5 μm (Figure 4H and Supplemental Figure S4I). However, it is possible that during contact guidance, the spatial constraints of adhesive cues are sufficient to organize adhesion and direct protrusions.

Together these results further demonstrate that both the area and orientation of lamellipodial protrusions contribute to contact guidance. The poorest contact guidance occurs in cells with reduced orientation, such as what occurs in ROCK-inhibited or RacQ61L-expressing cells (Figure 4, G and H). Alternatively, contact guidance can be improved over the WT condition by reduced overall lamellipodial size and improved orientation.

DISCUSSION

The ability of cells to change shape and direct their migration in response to ECM geometric cues has been characterized for decades and remains an area of active research (Dunn and Ebendal, 1978; Nakatsuji *et al.*, 1982; Dickinson *et al.*, 1994; den Braber *et al.*, 1996a; Teixeira *et al.*, 2003; Xia *et al.*, 2008). Previous studies characterized extensively the ability of a variety of cells to respond to changes in ECM geometry at scales ranging from nanometers (Teixeira *et al.*, 2006; Loesberg *et al.*, 2007; Jang *et al.*, 2010) to hundreds of micrometers (Vedula *et al.*, 2012, 2014). Despite numerous studies that pointed that the ability of cells to sense their underlying matrix is ubiquitous across cell types and occurs at different scales, few studies addressed the mechanisms of contact guidance. Efforts focused on understanding the mechanisms of contact guidance in the extreme case in which cells are confined to a single line of ECM. In this case, cells move 1.5 times faster than in a classical two-dimensional environment due to changes in lamellipodial dynamics and increased mechanical coupling between adhesions and the protrusive machinery (Doyle *et al.*, 2009, 2012). Although the effects of different degrees of confinement on cell migration can be studied by varying the width of the ECM line, migration direction is trivially parallel to the ECM. Therefore, to understand the mechanisms by which cells adjust their direction of migration in response to changes in ECM geometry, we patterned microenvironments in which the ECM line width was constant. By patterning ECM architectures with parallel lines of a fixed width that impose no limitations on adhesion formation, we show that in the absence of confinement, cells are capable of directing migration parallel to the ECM.

Studies on cell-derived matrices and ECM protein hydrogels showed that cells orient their motility and shape in response to anisotropies in the ECM in the absence of confinement (Provenzano *et al.*, 2008; Kutys and Yamada, 2014). These experimental systems resemble more closely the in vivo microenvironment but have the disadvantage that it is challenging to control the degree of anisotropy of the ECM with subcellular resolution. In these cases, only binary comparisons can be made (aligned ECM vs. not aligned ECM), making it impossible to discern whether cells are sensitive to a range of anisotropies in the ECM or guidance is just a binary phenomenon. By varying the spacing between lines, we are able to control the degree of anisotropy in the ECM. Thus our study addresses a gap in the literature, showing that variations in anisotropy of the ECM at the micrometer scale can influence migration in a continuous way. At the same time, we show that by changing the fibril-like spacing alone, cells can tune their guidance behavior, in contrast with previous studies, in which surface topography and fibril-like spacing were changed simultaneously (den Braber *et al.*, 1996a,b, 1998; Flemming *et al.*, 1999; van Kooten and von Recum, 1999; Walboomers *et al.*, 1999a,b; Matsuzaka *et al.*, 2000; Teixeira *et al.*, 2003; Provenzano *et al.*, 2008).

Our work provides the foundation for a mechanistic understanding of contact guidance at the micrometer scale. Previous work on structured ECM showed that Rac was activated at sites of adhesion formation and consequently stimulated protrusion formation at those sites (Xia *et al.*, 2008), whereas myosin II activity was important for the cell shape changes that occur in response to structured ECM (Frey *et al.*, 2006; Spedden *et al.*, 2014). However, by manipulating the main feedbacks that regulate cell migration, we show that defects in contact guidance stem from defects in the spatial control of protrusive activity. Our quantitative analysis enabled the characterization of contact guidance, allowing comparison of cellular phenotypes across different perturbations. Comparison across experimental conditions shows that perturbations by which cells lose their ability to migrate parallel to the ECM fail to localize protrusions (compare Figures 3J and 4H) or have protrusions with increased area (compare Figures 3J and 4G). By contrast, Arp 2/3 inhibition improves contact guidance by a decreasing the protrusion area (compare Figures 3J and 4G) and improving localization of protrusions along the lines. Collectively, these results show that contact guidance relies on spatial control of leading-edge protrusion.

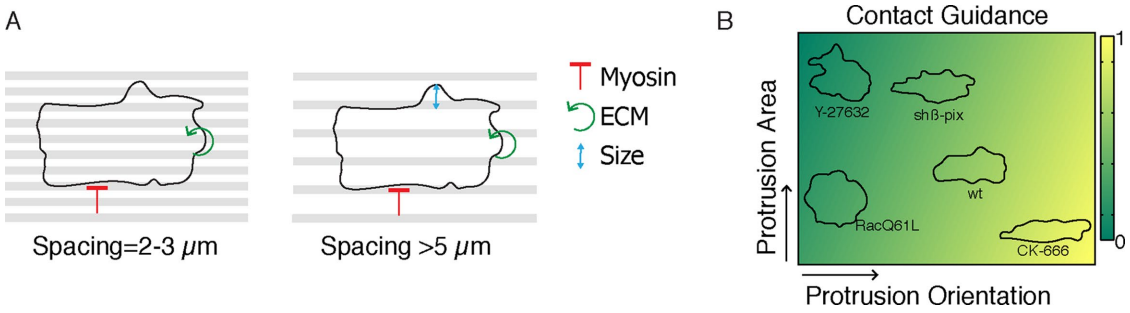

FIGURE 5: (A) Schematic representation of feedbacks that regulate protrusion area and orientation during contact guidance. At line spacings ≤5 μm, myosin II contractility inhibits protrusion from straight edges, and activation of Rac at adhesions promotes protrusion initiation parallel to the ECM. At spacings ≥5 μm, constraints in lamellipodia size limit stabilization of protrusions perpendicular to the ECM, promoting further contact guidance. (B) Schematic representation of the model for contact guidance. The guidance response depends on two protrusion physical parameters: area and orientation.

The defects we observe in migration guidance can be explained by changes in two distinct parameters of protrusion: orientation and size. Specifically, contact guidance is controlled by each of these parameters; disruption of either one is sufficient to produce loss of contact guidance. These two parameters are tuned subcellularly by positive feedback between adhesion formation and protrusion initiation and negative feedback between myosin II–dependent elongated shapes and formation of protrusions perpendicular to the ECM. For spacings ≤5 μm, these two feedbacks are required to enforce elongated cell shapes and migration to the ECM. As spacing is increased, the physical size of protrusions limits the ability of protrusions to be stabilized perpendicular to the ECM, further enhancing contact guidance (Figure 5A). The spacing at which this transition occurs is most likely cell-type dependent because variations in lamellipodia size that are cell-type dependent will influence this. Thus we envision that contact guidance is a function of protrusion area and orientation, where these two parameters can be regulated through different cellular pathways (Figure 5B). Future work needs to investigate other cellular pathways that regulate the efficiency of contact guidance that may arise from focal adhesion signaling and protrusion dynamics. In addition, the connection between contact guidance at the micrometer and nanometer scales remains to be explored. Although there is little mechanistic understanding of contact guidance at the nanometer scale, there is evidence that focal adhesion and protrusion orientation correlate with the ability of cells to align parallel to the underlying matrix (Teixeira *et al.*, 2003, 2006; Jang *et al.*, 2010). At this scale, other molecular feedbacks might become important for ECM sensing, such as local curvature of cell shape and adhesion signaling driven by focal adhesion kinase (Houk *et al.*, 2012; Teo *et al.*, 2013).

MATERIALS AND METHODS

Cell culture and reagents

NIH 3T3 fibroblasts (American Type Culture Collection, Manassas, VA) were cultured in DMEM (Mediatech, Herndon, VA) and supplemented with 10% fetal bovine serum (HyClone; Thermo Fisher Scientific, Hampton, NH), 2 mM L-glutamine (Invitrogen, Carlsbad, CA), and penicillin-streptomycin (Invitrogen). The ARP2/3 inhibitor CK-666 and control compound CK-689 were purchased from Calbiochem. Y-27632 was purchased from Sigma-Aldrich. Cells were plated for 4 h and then incubated for 3 h in CK-666 or 45 min in Y-27632 before imaging or fixation at the concentration indicated for all experiments. Cells were transiently transfected with plasmid DNA constructs encoding GFP-stargazin (a gift from A. Karginov, University of Illinois at Chicago, Chicago, IL) and RacQ61L (a gift from the Gary Borisy laboratory, Northwestern University). Transfections were performed using a Neon electroporation system (Invitrogen). Short hairpin RNA (shRNA) construct sets for mouse β-pix (GIPZ Arhgef7 shRNA set) were purchased from Dharmacon through Thermo Fisher Scientific. Transfection of constructs was performed using a Neon electroporation system (Invitrogen). Puromycin and fluorescence selections of expressing cells were performed per the manufacturer's protocols. Knockdown efficiency was determined by Western blotting (Supplemental Figure S3), and a stable cell line was maintained for the V3LMM_521424 clone.

Western blot analysis

For Western blotting, cells were lysed in radioimmunoprecipitation assay buffer (50 mM Tris, 150 mM NaCl, 0.1 SDS, 0.5 Na deoxycholate, 1 Triton X-100, 1 mM phenylmethylsulfonyl fluoride, and protease inhibitor). Lysates were separated by SDS–PAGE gel and electrotransferred to a nitrocellulose membrane.

Blots were blocked in Odyssey blocking buffer and incubated with primary antibody (rabbit anti–β-pix; 07-1450-I, EMD Millipore; rabbit anti–glyceraldehyde-3-phosphate dehydrogenase; G9545, Sigma-Aldrich) overnight at 4°C. Blots were incubated in secondary antibody donkey anti–rabbit 680LT (C50224-04; Odyssey) for 1 h at room temperature. Blots were scanned using the Odyssey Fc imaging system and analyzed using the gel analysis tool in ImageJ (1.51f; National Institutes of Health).

Immunofluorescence

Cells were rinsed in warm cytoskeleton buffer (10 mM 2-(*N*-morpholino)ethanesulfonic acid, 3 mM $MgCl_2$, 1.38 M KCl, and 20 mM ethylene glycol tetraacetic acid) and then fixed and permeabilized in 4% paraformaldehyde (Electron Microscopy Sciences, Hatfield, PA), 1.5% bovine serum albumin (Thermo Fisher Scientific), and 0.5% Triton X-100 in cytoskeleton buffer for 15 min at 37°C. Coverslips were then rinsed three times in phosphate-buffered saline (PBS) and incubated with Alexa Fluor 488–phalloidin (1:800; Invitrogen), mouse anti-paxillin (1:400; Millipore), and rabbit anti-fibronectin (1:400; Sigma-Aldrich) overnight at 4°C. The coverslips were then rinsed three times in PBS and incubated for 1 h with an Alexa Fluor 647 donkey anti-mouse (1:800; Invitrogen) or Alexa Fluor 568 goat anti-rabbit (1:400; Invitrogen) secondary antibody. Coverslips were mounted on glass slides using the SlowFade Antifade kit (Invitrogen).

Micropatterning

Micropatterning via deep-ultraviolet (UV) illumination on polyacrylamide gels was done according to Oakes *et al.* (2014). Briefly, a chrome-plated quartz photomask (Microtronics, Newtown, PA) was cleaned with water and wiped with 0.5 ml of hexane (Sigma-Aldrich). A polyacrylamide gel mixture (7.5/0.3% weight percentage of acrylamide/bis-acrylamide) was polymerized for 30 min between the photomask and an activated glass coverslip, yielding a gel with a shear elastic modulus of 8.6 kPa. Once the gel was polymerized, the photomask was placed in a UVO-Cleaner 342 (Jelight, Irvine, CA) and illuminated with a combination of 185- and 254-nm UV light for 120 s. The coverslip and gel were then detached from the photomask by submerging the entire complex in water and gently lifting a corner of the coverslip with a tweezers. Gels were incubated in a solution containing 5 mg/ml EDC (Thermo Fisher Scientific) and 10 mg/ml NHS (Thermo Fisher Scientific) for 15 min. The EDC-NHS solution was then aspirated and replaced with a solution containing 10 μg/ml fibronectin in a buffer of 4-(2-hydroxyethyl)-1-piperazineethanesulfonic acid (HEPES; pH 8.5) for 20 min. Gels were washed with PBS and incubated overnight in DMEM before cells were plated.

Microscopy and live-cell imaging

For time-lapse imaging of migration, coverslips were mounted in a custom-made chamber made from galvanized aluminum with six 22-mm-diamater holes. Vacuum grease was used to affix several round coverslips to this chamber to facilitate time-lapse imaging of multiple coverslips simultaneously. Imaging media was supplemented with 10 mM HEPES and 30 ml/ml Oxyrase (Oxyrase, Mansfield, OH). Imaging of migration and spreading was performed on a temperature-controlled inverted Nikon (Melville, NY) Ti-E microscope with a Lumen 200 Pro light source (Prior) and an HQ2 cooled charge-coupled device (CCD) camera (Roper Scientific, Trenton, NJ) controlled via MetaMorph acquisition software (Molecular Devices, Eugene, OR). Images were acquired using a 20 or 10×/0.75 numerical aperture (NA) Plan Fluor air objective (Nikon).

Fluorescence images (fixed and live-cell imaging) were obtained on an inverted microscope (Ti-E; Nikon) with a confocal scan head (CSU-X; Yokogawa Electric, Musashino, Tokyo, Japan), laser merge module containing 491-, 561-, and 642-nm laser lines (Spectral Applied Research, Richmond Hill, Canada), and HQ2 CCD camera (Roper Scientific). MetaMorph acquisition software was used to control the microscope hardware. Images were acquired using a 60×/1.2 NA Plan Apo water-immersion objective, a 20×/0.75 NA Plan Fluor multi-immersion objective (Nikon), or a 20× Plan Fluor air objective.

Analysis of cell shape and motion

F-actin images were thresholded in MATLAB to obtain a mask representing the cell. The built-in "regionprops" function was used to fit an ellipse to each cell mask and obtain its major (*b*) and minor (*a*) axes. Cell shape elongation was defined by the ratio *b*/*a*. Orientation was defined as $P = \cos^2\theta$, where θ is the angle between a line parallel to the ECM and the long axis, *b*, of the cell ellipse. The average was calculated over all of the cells on a given ECM pattern imaged for each condition ($N > 50$).

Cells were manually tracked using the manual tracking plug-in in ImageJ. Instantaneous speed was measured from cell displacements at 20-min intervals. Mean cell speed was calculated by averaging instantaneous cell speed over a period of 10 h. To assess directionality of migration, we analyzed cell trajectories over a period of 10 h. For each time step in a trajectory, we calculated the angle θ between the displacement vector of a cell and the ECM. We defined a guidance parameter *g* such that

$$g(t) = \begin{cases} 0 & \text{if } \theta < 25 \\ 1 & \text{if } \theta \geq 25 \end{cases}$$

for every displacement in a cell's trajectory. Once we obtained guidance values, we calculated the mean guidance as a function of lag time:

$$G(\tau) = \sum_{t=t_i}^{t_i+\tau} g(t) / \tau$$

We reported the guidance value obtained at $\tau = 300$ because around this value the curves ceased to increase (Supplemental Figure S1B).

Protrusion measurements

To determine the area and direction of protrusive fronts, we obtained contours of each cell by thresholding GFP-stargazin imaging. From the contours, we extracted protrusions using custom MATLAB software to identify the regions of area growth from between contours at times *t* and *t* + 2 min. Once protrusive regions were identified, we determined their orientation with respect to the ECM pattern by calculating $P = \cos^2\theta$, where θ is the angle between a line parallel to the ECM and the line defined by the centroid of the cell and the centroid of the protrusive region. The average was taken over the angles of all cellular protrusions that occur in a 30-min time interval. Because ECM patterns are symmetric with respect to the *y*-axis, angles > 90° were reflected across the y-axis such that $\theta \in [0, 90]$. Areas of protrusions were obtained using the regionprops function in MATLAB.

Statistical analysis and data reproducibility

The data for all the plots shown, with the exception of Supplemental Figure S3, D, E, G, and H, were obtained from at least two independent experiments. Supplemental Table S1 shows the number of replicates for the data in each figure. There were no limitations on data reproducibility. Exact sample sizes (*N* values) for all of the plots included in the figures are shown in Supplemental Table S2. Pairwise *t* tests were used to determine whether variables measured at different line spacings were statistically significant from each other. Post hoc analysis using the Holm method was used to correct for multiple pairwise comparisons. Welch's *t* tests were used to determine whether the data from two experimental conditions at the same line spacing were significantly different. Exact *p* values for all tests are shown in Supplemental Table S3. All statistical analyses were performed using R software (RStudio Version 1.0.136).

ACKNOWLEDGMENTS

We thank Yvonne Beckham for assistance with molecular biology. We are also grateful to Barbara Hissa and Bob Harmon for assistance with Western blotting and to Tim Fessenden for critical comments on the figures. This work was supported by a National Science Foundation Graduate Research Fellowship to G.R.R-SJ. and National Institutes of Health Grant R01GM104032 to M.L.G.

REFERENCES

Baker BM, Chen CS (2012). Deconstructing the third dimension: how 3D culture microenvironments alter cellular cues. J Cell Sci 125, 3015–3024.

Beckham Y, Vasquez RJ, Stricker J, Sayegh K, Campillo C, Gardel ML (2014). Arp2/3 inhibition induces amoeboid-like protrusions in MCF10A epithelial cells by reduced cytoskeletal-membrane coupling and focal adhesion assembly. PLoS One 9, e100943.

Brownfield DG, Venugopalan G, Lo A, Mori H, Tanner K, Fletcher DA, Bissell MJ (2013). Patterned collagen fibers orient branching mammary epithelium through distinct signaling modules. Curr Biol 23, 703–709.
Cai Y, Rossier O, Gauthier NC, Biais N, Fardin MA, Zhang X, Miller LW, Ladoux B, Cornish VW, Sheetz MP (2010). Cytoskeletal coherence requires myosin-IIA contractility. J Cell Sci 123, 413–423.
Charras G, Sahai E (2014). Physical influences of the extracellular environment on cell migration. Nat Rev Mol Cell Biol 15, 813–824.
Clark P, Connolly P, Curtis AS, Dow JA, Wilkinson CD (1990). Topographical control of cell behaviour: II. Multiple grooved substrata. Development 108, 635–644.
Condeelis J, Segall JE (2003). Intravital imaging of cell movement in tumours. Nat Rev Cancer 3, 921–930.
den Braber ET, de Ruijter JE, Ginsel LA, von Recum AF, Jansen JA (1996a). Quantitative analysis of fibroblast morphology on microgrooved surfaces with various groove and ridge dimensions. Biomaterials 17, 2037–2044.
den Braber ET, de Ruijter JE, Ginsel LA, von Recum AF, Jansen JA (1998). Orientation of ECM protein deposition, fibroblast cytoskeleton, and attachment complex components on silicone microgrooved surfaces. J Biomed Mater Res 40, 291–300.
den Braber ET, de Ruijter JE, Smits HT, Ginsel LA, von Recum AF, Jansen JA (1996b). Quantitative analysis of cell proliferation and orientation on substrata with uniform parallel surface micro-grooves. Biomaterials 17, 1093–1099.
Dickinson RB, Guido S, Tranquillo RT (1994). Biased cell migration of fibroblasts exhibiting contact guidance in oriented collagen gels. Ann Biomed Eng 22, 342–356.
Doyle AD, Kutys ML, Conti MA, Matsumoto K, Adelstein RS, Yamada KM (2012). Micro-environmental control of cell migration–myosin IIA is required for efficient migration in fibrillar environments through control of cell adhesion dynamics. J Cell Sci 125, 2244–2256.
Doyle AD, Wang FW, Matsumoto K, Yamada KM (2009). One-dimensional topography underlies three-dimensional fibrillar cell migration. J Cell Biol 184, 481–490.
Dunn GA, Ebendal T (1978). Contact guidance on oriented collagen gels. Exp Cell Res 111, 475–479.
Dunn GA, Heath JP (1976). A new hypothesis of contact guidance in tissue cells. Exp Cell Res 101, 1–14.
Elliott H, Fischer RS, Myers KA, Desai RA, Gao L, Chen CS, Adelstein RS, Waterman CM, Danuser G (2015). Myosin II controls cellular branching morphogenesis and migration in three dimensions by minimizing cell-surface curvature. Nat Cell Biol 17, 137–147.
Flemming RG, Murphy CJ, Abrams GA, Goodman SL, Nealey PF (1999). Effects of synthetic micro- and nano-structured surfaces on cell behavior. Biomaterials 20, 573–588.
Frey MT, Tsai IY, Russell TP, Hanks SK, Wang YL (2006). Cellular responses to substrate topography: role of myosin II and focal adhesion kinase. Biophys J 90, 3774–3782.
Friedl P, Gilmour D (2009). Collective cell migration in morphogenesis, regeneration and cancer. Nat Rev Mol Cell Biol 10, 445–457.
Gabella C, Bertseva E, Bottier C, Piacentini N, Bornert A, Jeney S, Forró L, Sbalzarini IF, Meister JJ, Verkhovsky AB (2014). Contact angle at the leading edge controls cell protrusion rate. Curr Biol 24, 1126–1132.
Gardel ML, Schneider IC, Aratyn-Schaus Y, Waterman CM (2010). Mechanical integration of actin and adhesion dynamics in cell migration. Annu Rev Cell Dev Biol 26, 315–333.
Gillitzer R, Goebeler M (2001). Chemokines in cutaneous wound healing. J Leukoc Biol 69, 513–521.
Houk AR, Jilkine A, Mejean CO, Boltyanskiy R, Dufresne ER, Angenent SB, Altschuler SJ, Wu LF, Weiner OD (2012). Membrane tension maintains cell polarity by confining signals to the leading edge during neutrophil migration. Cell 148, 175–188.
James J, Goluch ED, Hu H, Liu C, Mrksich M (2008). Subcellular curvature at the perimeter of micropatterned cells influences lamellipodial distribution and cell polarity. Cell Motil Cytoskeleton 65, 841–852.
Jang KJ, Kim MS, Feltrin D, Jeon NL, Suh KY, Pertz O (2010). Two distinct filopodia populations at the growth cone allow to sense nanotopographical extracellular matrix cues to guide neurite outgrowth. PLoS One 5, e15966.
Keller R (2005). Cell migration during gastrulation. Curr Opin Cell Biol 17, 533–541.
King SJ, Asokan SB, Haynes EM, Zimmerman SP, Rotty JD, Alb JG, Tagliatela A, Blake DR, Lebedeva IP, Marston D, *et al.* (2016). Lamellipodia are crucial for haptotactic sensing and response. J Cell Sci 129, 2329–2342.
Kutys ML, Yamada KM (2014). An extracellular-matrix-specific GEF-GAP interaction regulates Rho GTPase crosstalk for 3D collagen migration. Nat Cell Biol 16, 909–917.
Lauffenburger DA, Horwitz AF (1996). Cell migration: a physically integrated molecular process. Cell 84, 359–369.
Lehnert D, Wehrle-Haller B, David C, Weiland U, Ballestrem C, Imhof BA, Bastmeyer M (2004). Cell behaviour on micropatterned substrata: limits of extracellular matrix geometry for spreading and adhesion. J Cell Sci 117, 41–52.
Lo CM, Buxton DB, Chua GC, Dembo M, Adelstein RS, Wang YL (2004). Nonmuscle myosin IIb is involved in the guidance of fibroblast migration. Mol Biol Cell 15, 982–989.
Lo CM, Wang HB, Dembo M, Wang YL (2000). Cell movement is guided by the rigidity of the substrate. Biophys J 79, 144–152.
Loesberg WA, te Riet J, van Delft FC, Schön P, Figdor CG, Speller S, van Loon JJ, Walboomers XF, Jansen JA (2007). The threshold at which substrate nanogroove dimensions may influence fibroblast alignment and adhesion. Biomaterials 28, 3944–3951.
Londono C, Loureiro MJ, Slater B, Lücker PB, Soleas J, Sathananthan S, Aitchison JS, Kabla AJ, McGuigan AP (2014). Nonautonomous contact guidance signaling during collective cell migration. Proc Natl Acad Sci USA 111, 1807–1812.
Luster AD, Alon R, von Andrian UH (2005). Immune cell migration in inflammation: present and future therapeutic targets. Nat Immunol 6, 1182–1190.
Machacek M, Hodgson L, Welch C, Elliott H, Pertz O, Nalbant P, Abell A, Johnson GL, Hahn KM, Danuser G (2009). Coordination of Rho GTPase activities during cell protrusion. Nature 461, 99–103.
Matsuzaka K, Walboomers F, de Ruijter A, Jansen JA (2000). Effect of microgrooved poly-l-lactic (PLA) surfaces on proliferation, cytoskeletal organization, and mineralized matrix formation of rat bone marrow cells. Clin Oral Implants Res 11, 325–333.
Mogilner A, Keren K (2009). The shape of motile cells. Curr Biol 19, R762–R771.
Nakatsuji N, Gould AC, Johnson KE (1982). Movement and guidance of migrating mesodermal cells in Ambystoma maculatum gastrulae. J Cell Sci 56, 207–222.
Nayal A, Webb DJ, Brown CM, Schaefer EM, Vicente-Manzanares M, Horwitz AR (2006). Paxillin phosphorylation at Ser273 localizes a GIT1-PIX-PAK complex and regulates adhesion and protrusion dynamics. J Cell Biol 173, 587–589.
Nobes CD, Hall A (1999). Rho GTPases control polarity, protrusion, and adhesion during cell movement. J Cell Biol 144, 1235–1244.
Oakes PW, Banerjee S, Marchetti MC, Gardel ML (2014). Geometry regulates traction stresses in adherent cells. Biophys J 107, 825–833.
Omelchenko T, Rabadan MA, Hernández-Martínez R, Grego-Bessa J, Anderson KV, Hall A (2014). β-Pix directs collective migration of anterior visceral endoderm cells in the early mouse embryo. Genes Dev 28, 2764–2777.
Omelchenko T, Vasiliev JM, Gelfand IM, Feder HH, Bonder EM (2002). Mechanisms of polarization of the shape of fibroblasts and epitheliocytes: separation of the roles of microtubules and Rho-dependent actin-myosin contractility. Proc Natl Acad Sci USA 99, 10452–10457.
Pankov R, Endo Y, Even-Ram S, Araki M, Clark K, Cukierman E, Matsumoto K, Yamada KM (2005). A Rac switch regulates random versus directionally persistent cell migration. J Cell Biol 170, 793–802.
Parker KK, Brock AL, Brangwynne C, Mannix RJ, Wang N, Ostuni E, Geisse NA, Adams JC, Whitesides GM, Ingber DE (2002). Directional control of lamellipodia extension by constraining cell shape and orienting cell tractional forces. FASEB J 16, 1195–1204.
Petrie RJ, Doyle AD, Yamada KM (2009). Random versus directionally persistent cell migration. Nat Rev Mol Cell Biol 10, 538–549.
Price LS, Leng J, Schwartz MA, Bokoch GM (1998). Activation of Rac and Cdc42 by integrins mediates cell spreading. Mol Biol Cell 9, 1863–1871.
Provenzano PP, Inman DR, Eliceiri KW, Trier SM, Keely PJ (2008). Contact guidance mediated three-dimensional cell migration is regulated by Rho/ROCK-dependent matrix reorganization. Biophys J 95, 5374–5384.
Raftopoulou M, Hall A (2004). Cell migration: Rho GTPases lead the way. Dev Biol 265, 23–32.
Reig G, Pulgar E, Concha ML (2014). Cell migration: from tissue culture to embryos. Development 141, 1999–2013.
Ridley AJ, Schwartz MA, Burridge K, Firtel RA, Ginsberg MH, Borisy G, Parsons JT, Horwitz AR (2003). Cell migration: integrating signals from front to back. Science 302, 1704–1709.
Spedden E, Wiens MR, Demirel MC, Staii C (2014). Effects of surface asymmetry on neuronal growth. PLoS One 9, e106709.

Sun X, Driscoll MK, Guven C, Das S, Parent CA, Fourkas JT, Losert W (2015). Asymmetric nanotopography biases cytoskeletal dynamics and promotes unidirectional cell guidance. Proc Natl Acad Sci USA 112, 12557–12562.
Teixeira AI, Abrams GA, Bertics PJ, Murphy CJ, Nealey PF (2003). Epithelial contact guidance on well-defined micro- and nanostructured substrates. J Cell Sci 116, 1881–1892.
Teixeira AI, McKie GA, Foley JD, Bertics PJ, Nealey PF, Murphy CJ (2006). The effect of environmental factors on the response of human corneal epithelial cells to nanoscale substrate topography. Biomaterials 27, 3945–3954.
Teo BK, Wong ST, Lim CK, Kung TY, Yap CH, Ramagopal Y, Romer LH, Yim EK (2013). Nanotopography modulates mechanotransduction of stem cells and induces differentiation through focal adhesion kinase. ACS Nano 7, 4785–4798.
van Kooten TG, von Recum AF (1999). Cell adhesion to textured silicone surfaces: the influence of time of adhesion and texture on focal contact and fibronectin fibril formation. Tissue Eng 5, 223–240.
Vasilyev A, Liu Y, Mudumana S, Mangos S, Lam PY, Majumdar A, Zhao J, Poon KL, Kondrychyn I, Korzh V, Drummond IA (2009). Collective cell migration drives morphogenesis of the kidney nephron. PLoS Biol 7, e9.
Vedula SR, Hirata H, Nai MH, Brugués A, Toyama Y, Trepat X, Lim CT, Ladoux B (2014). Epithelial bridges maintain tissue integrity during collective cell migration. Nat Mater 13, 87–96.
Vedula SR, Leong MC, Lai TL, Hersen P, Kabla AJ, Lim CT, Ladoux B (2012). Emerging modes of collective cell migration induced by geometrical constraints. Proc Natl Acad Sci USA 109, 12974–12979.
Walboomers XF, Croes HJ, Ginsel LA, Jansen JA (1999a). Contact guidance of rat fibroblasts on various implant materials. J Biomed Mater Res 47, 204–212.
Walboomers XF, Monaghan W, Curtis AS, Jansen JA (1999b). Attachment of fibroblasts on smooth and microgrooved polystyrene. J Biomed Mater Res 46, 212–220.
Wang HR, Zhang Y, Ozdamar B, Ogunjimi AA, Alexandrova E, Thomsen GH, Wrana JL (2003). Regulation of cell polarity and protrusion formation by targeting RhoA for degradation. Science 302, 1775–1779.
Weiss P, Garber B (1952). Shape and movement of mesenchyme cells as functions of the physical structure of the medium: contributions to a quantitative morphology. Proc Natl Acad Sci USA 38, 264–280.
Wolfenson H, Iskratsch T, Sheetz MP (2014). Early events in cell spreading as a model for quantitative analysis of biomechanical events. Biophys J 107, 2508–2514.
Wu C, Asokan SB, Berginski ME, Haynes EM, Sharpless NE, Griffith JD, Gomez SM, Bear JE (2012). Arp2/3 is critical for lamellipodia and response to extracellular matrix cues but is dispensable for chemotaxis. Cell 148, 973–987.
Xia N, Thodeti CK, Hunt TP, Xu Q, Ho M, Whitesides GM, Westervelt R, Ingber DE (2008). Directional control of cell motility through focal adhesion positioning and spatial control of Rac activation. FASEB J 22, 1649–1659.
Yoon SH, Kim YK, Han ED, Seo YH, Kim BH, Mofrad MR (2012). Passive control of cell locomotion using micropatterns: the effect of micropattern geometry on the migratory behavior of adherent cells. Lab Chip 12, 2391–2402.